Identification of tracer clouds: A shape-based approach

Nilanjan Ray*, Dipti Prasad Mukherjee and Jyotirmoy Das

Electronics and Communication Sciences Unit, Indian Statistical Institute, Calcutta 700 035, India

Spatio-temporal life cycle of meteorological structures is an important part of study of routine numerical weather analysis. In this paper we present an algorithm to track tracer clouds in INSAT image sequence. Given a pair of sequence images taken at a 30 min interval, the objective of cloud tracking is to derive the path of movement of a cloud contour in the source image to the corresponding contour of the destination image. This has direct relevance to cloud motion vector (CMV) analysis by which wind speed and direction are estimated. We have utilized an improved algorithm to generate a set of initial estimates of possible cloud motion vectors which are then filtered through a shape-based approach. The contour of cloud mass is modelled as a perfectly flexible string, and depending on initial estimates of CMV, the source cloud contours are deformed. The CMV direction for which the deformed contour best matches the destination contour, gives the optimum path of cloud movement from source to destination image. The algorithm is demonstrated using images from INSAT.

EXTRACTION of Cloud Motion Vectors (CMVs) is part of an important routine synoptic scale weather study[1–3]. CMVs are detected in geo-stationary satellite (e.g. INSAT, GMS) images, and they provide wind speed and direction at given latitude–longitude coordinates. In conjunction to this, a study of the spatio-temporal life cycle of cloud mass is of typical consideration to meteorologists[4]. By spatio-temporal life cycle of the cloud, we mean the generation, dissipation and assimilation of clouds seen in a sequence of geo-stationary satellite pictures.

We relate the study of life cycle of the cloud to be essentially a problem of cloud tracking in a sequence of satellite images. From the computer vision point of view, this tracking of cloud images may be considered as the study of deformable shape. In day-to-day numerical weather predictions, tracer clouds are taken as candidates for cloud tracking and subsequent wind speed estimation analysis. The major characteristic of a tracer cloud is that it has comparatively higher form or shape stability over at least the period of observation (typically 30 min).

In this paper, we unfold a local computation-based algorithm for cloud tracking. For brevity of space, we will not go to the extent of utilizing this algorithm for CMV detection but point out the existing algorithms for CMV detection as well as cloud tracking and show how our process can give an alternate estimate of cloud tracking which is more appropriate for large cloud masses. Our proposed method of tracer cloud tracking is a two-stage process. In the first stage, a set of initial cloud motion vectors are detected using an intensity gradient-based approach[5–7]. In the second, these initial directional estimates are filtered using a shape (contour)-based approach. We conclude mentioning the relevant issues connected with this problem.

In the next section of this paper, the problem of cloud tracking is critically analysed. In addition, the existing CMV algorithms, their advantages and limitations are discussed. The existing deformable shape-modelling relevant to the cloud tracking problem is also described. Our proposed algorithm on cloud tracking is presented next. Some illustrations that qualitatively evaluate our proposed method are presented next. The last section reports our conclusions with a discussion on the proposed approach. The possible extension of our work is also mentioned.

A close look at the problem of cloud tracking

The specific issues associated with cloud tracking are as follows:

(i) Tracer clouds are detected in a source satellite image s taken at, say, time t. Given minor deformations over a time period δt (typically 30 min), the problem is to identify the same in destination image d taken at time $t + \delta t$. The INSAT images shown in this paper are also taken at 30 min intervals.

(ii) Establishing a point-to-point correspondence from the source cloud contour to the destination cloud contour. The result of tracking is then the minimum energy or cost path through which points of interest of the start contour deform to corresponding points of the destination contour.

We first discuss, in brief, the existing CMV detection methods to see how some of these issues are addressed therein. This would also act as a prerequisite to understand our cloud tracking algorithm.

The existing CMV algorithm

The process of CMV detection dates back to the early seventies[6–9] followed by its implementations in the India

*For correspondence

Meteorological Department[7,10] in the late eighties. Even recently, there are extensions and quality control initiatives of CMV studies not only with cloud images but with images from satellites equipped with water vapour channels[11,12]. The crux of such approaches has the following major steps:

- The cloud mass (or tracer cloud) whose displacement is detected in subsequent image frames is selected by meteorologists. This is mainly an expert-dependent process.
- The source image s and destination image d are registered to same scale (as they are taken from a single geostationary satellite over a time interval). For every given $m \times m$ (typically, 15×15 pixels) subimage c_s of the tracer cloud in image s, an $n \times n$ search window w_d is selected in d. Note that the centre coordinates of c_s and w_d are identical as s and d are registered to the same scale. Typically, the dimension of n is 37 for low clouds whereas it is 61 in the case of medium or high clouds.
- Given c_s and w_d, the problem of CMV detection is finding the best correlation measure between c_s and any one of $m \times m$ subimage within w_d. The vector originating from the centre coordinate of c_s to the centre of best matched $m \times m$ subimages of w_d gives the CMV. The process is explained in Figure 1.
- The correlation measures are some sort of similarity measure between time varying subimages. From that standpoint, the method is also known as (intensity) gradient-based approach, and the similarity measures are classified as: (i) Maximum cross-correlation measure (MCC)[13], (ii) Sum of absolute value difference measure (SAVD)[7,14], and (iii) Sum of squared difference measure (SSD)[15].

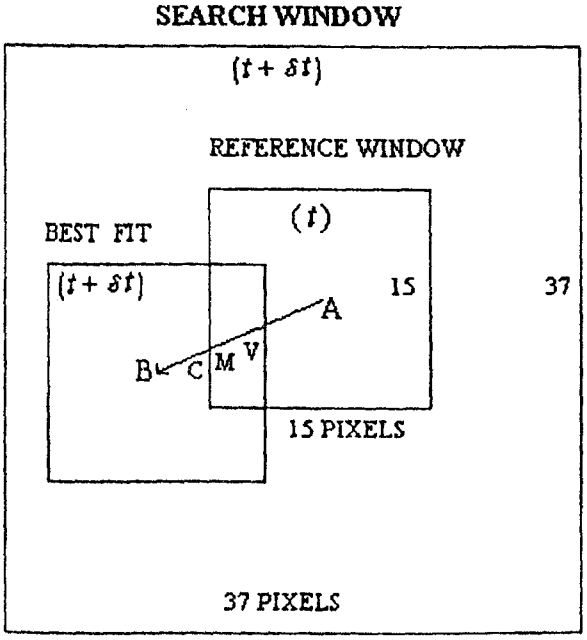

Figure 1. Schematic for cloud motion vector detection process.

Kelkar and Khanna[7] claimed that the sum of absolute difference between corresponding pixels of c_s and 15×15 subimage of w_d ($\Sigma_0^{224} |x - y|$, x is a pixel of c_s and y is the corresponding pixel of 15×15 subimage of w_d) is a good and computationally attractive yardstick compared to cross-correlation measure $((\overline{xy}/\sigma_x\sigma_y) - (\Sigma xy/N\sigma_x\sigma_y)$, $N = 225$) originally proposed by Lease and Novak[6].

The correlation-based approaches are by and large adopted by different operational agencies[2,3] for routine numerical weather prediction because of computational simplicity. Also, CMV detection is always subject to quality control by expert meteorologists where, inconsistent CMVs are manually removed. However, this process has its limitation in that in a dynamic situation of meteorological nature the correlation surface between the source subimage c_s and the candidate subimage within w_d is typically multimodal and unimodal only in very special cases. Such a matching technique also has an implicit assumption of rigidity in the form of the cloud mass. However, in reality, the clouds not only get translated, rotated, sheared but also deformed in temporal scale. Such problems could be eliminated to a large extent if images could be acquired at a very high temporal rate. Unfortunately, for practical operational constraints, frame grabbing at such an increased speed is not possible (except during severe cyclonic disturbances).

To improve this aspect, various quality control initiatives[16] of CMV detection are being undertaken. For example, there are energy-based approaches, specifically gabor energy filters[17,18] to extract motion information. The major limitation in such cases is the requirement of a large number of sequence images at shorter intervals. Also there are several feature-based approaches[19] which primarily focus on invariant features in time-varying images; but for most cases, an implicit shape rigidity is assumed. In a different context, an excellent review of shape from motion is provided by Agarwal and Nandhakumar[20]; however, even though it surveys a number of gradient-based approaches, the issue of shape deformability is not addressed in detail.

We discuss a hybrid approach proposed by Wu[5] as it has relevance to our work detailed in the section 'proposed method'. This hybrid approach improves correlation estimates after incorporating a relaxation labelling algorithm[21]. For a $p \times p$ subimage of s, his model is given by:

$$f(x,y) = a \cdot g(x,y;u,v) + m + n, \quad 1 \le x,y \le p, \qquad (1)$$

where $f(x, y)$ is basically the c_s mentioned earlier and $g(x, y; u, v)$ is the (u, v) shifted version of $f(x, y)$ within the search space w_d. The factor a is a scale factor considering the change in image contrast in δt time, m is a mean bias in modelling intensity, and n is a typical zero-mean gaussian noise. He has derived that the similarity measure between c_s and the candidate in w_d depends on a factor $i(u, v)$:

$$i(u,v) = \sum\sum((f(x,y)-\bar{f})-(g(x,y;u,v)-\bar{g}(u,v)))^2. \quad (2)$$

Interested readers can refer to Wu[5] for a detailed derivation. For every point of interest in image s and the corresponding w_d, he detects a set of CMVs. Each of such CMVs is associated with a probability value which is the similarity or normalized correlation measure between $f(x, y)$ and $g(x, y; u, v)$. CMVs with a correlation measure less than a threshold are rejected outright. However, the major contribution of his approach is in updating these probability values in an iterative process where consistency between two neighbouring vector directions is utilized. The iterative process follows the relaxation labelling algorithm described by Rosenfeld and Kak[21]. Since the neighbouring CMV direction consistency has been taken care of in this algorithm, he has got attractive results even in the case of cyclonic storms where shape stability is very poor.

The problem in extending this algorithm to cloud tracking is that it does not incorporate any shape-based features. The fragmented cloud regions of interest in his experiment[5] is a few pixels wide. Note that typically, for geo-stationary satellites like INSAT, each pixel resolution represents 2–8 km on earth (depending on visible or IR band). The assumption of CMV directional consistency over such a small region of fragmented cloud cover is tenable. However, such a directional consistency over a relatively large cloud tracer, used in routine day-to-day cloud tracking operations, may not be a safe assumption. Moreover, a large cloud tracer, because of shape deformation, can result in *false correspondence* between images s and d.

In our proposed cloud-tracking algorithm, we show a variation of the correlation measure of Wu[5] to generate an initial estimate of motion of contour of tracer cloud. Subsequently we present a shape-based matching criterion between the parts of contour of source and that of destination tracer cloud. In this context let us review the existing cloud-tacking approach which has direct relevance to our algorithm. We also explore how the problem of deformable shape is tackled in similar cases. Our objective is not to address all the literature which deals with deformable shape in a set of sequence image, but to discuss only that which is relevant to our work.

Deformable shape modelling in the context of cloud tracking

Two specific approaches are relevant in the context of cloud tracking.

- There is a whole bunch of *snake*-based approach[22–27] where, in general, either an initial contour is detected or a seed contour is made to take the shape of the contour to be tracked after minimizing energy corresponding to the profile of the shape boundary.
- In a different approach[28], a set of shape invariant points or 'point landmarks' are located in the boundary. These points are generally at a high curvature on the contour. It is assumed that deformation is marginal at or close to the high curvature points. This is certainly true for images of deformable biological organs[28]. In the absence of any active meteorological phenomenon, high curvature points in satellite images at a 30 min rate have higher form stability compared to the rest of the contour. We utilize this assumption while dealing with our tracking problem.

Tracking of meteorological structures, namely clouds, through curve matching first proposed by Cohen and Herlin[29] assumes that the flow of source contour to the destination contour takes place along a minimum cost path. The source and destination areas are presented using level sets[30]. The shortest path between two points on a surface is defined by the minimal geodesic. The tracking path from the source contour to the destination contour is characterized by the minimal cost path. The optimum cost path p^{opt} is defined by:

$$C(p^{opt}_{X_s}) = \min_{p_{X_s}} C(p_{X_s}), \quad (3)$$

where

$$C(p_{X_s}) = \int_{X_s}^{X_d} c(x, y)\, ds,$$

p_{X_s} is the path from the source contour point X_s to matching point X_d on the destination contour. Evaluation of p^{opt} is then the minimization of a cost function $c(x, y)$. Cohen and Herlin[29] have defined this cost function as a combination of distance maps of the source and the destination contours. In this context they have mentioned: 'A more elaborate model should take into account the geometrical properties of the curve, for example, curvature information in a small neighbourhood of the source and destination areas'.

Proposed method

In our proposed model, we utilize a variation of cross-correlation measure proposed by Wu[5] to detect a set of possible directional vectors on source contour points along which possible movement of source contour points have occurred. Then a shape-based cost function is used to find the best direction among these along which contour displacement has taken place from source to destination. It uses a combination of gradient-based approach followed by filtering using shape-based approach. It avoids the directional consistency assumption proposed by Wu[5] and adds on geometrical properties of the contour which is lacking in Cohen and Herlin's approach[29]. It also avoids the complex geodesic calculation as in Cohen and Herlin's approach[29].

Our proposed algorithm is outlined as follows. We start with source and destination contours, c_r and c_d respectively, of the tracer cloud. The contours of individual cloud clusters are obtained applying an active contour model, called *g-snake* as proposed by Lai and Chin[24,25]. Since border detection is not the prime objective, we avoid the detailed implementation as it is available in literature[24].

- A snake-following algorithm coupled with split and merge of linear and curvilinear segments is applied on c_r to detect the set of control points on the contour[31]. Note that all significant points on the contour including high curvature points will be selected as vertices of the guiding polygon. Coordinates of all the guiding polygon vertices are stored in a vertex table.
- For every entry v_i in the vertex table, a $p \times p$ mask $f(x, y)$ is considered centred around the vertex v_i. A search window w_d of radius V_m is assumed in destination image d. The centre of w_d corresponds to the coordinate of v_i of c_r. Similar to CMV detection process, a similarity measure is established for every $p \times p$ mask inside w_d with the $p \times p$ mask centered around v_i of c_r. We have used the following similarity measure given by:

$$i(u,v) = \sum\sum (f(x,y) - g(x,y;u,v))^2. \quad (4)$$

This is computationally simpler than the measure in eq. (2). Since the resultant direction vector is filtered through shape-based matching in the next step, our emphasis is on generating as many direction vectors as possible in the shortest possible time.

Note that the similarity measure is thresholded at p such that all directional vectors with similarity measure greater than p are outright rejected. The result of this step is a set of direction vectors at every vertex of the guiding polygon of c_r. This is demonstrated in Figure 2 *a*.

- For every vertex v_i of the vertex table, vertices v_{i-1} and v_{i+1} are indexed. Surface normals N_{i-1} and N_{i+1} are drawn from v_{i-1} and v_{i+1}, respectively. Contours between v_{i-1} and v_{i+1} of c_r and I_{i-1} and I_{i+1} of c_d are considered for shape-based matching. The process is shown in Figure 2 *c*. We do not assume the entire contour between v_{i-1} and v_{i+1} of c_r to be transformed to I_{i-1} and $I_{i+1}$of c_d; but given the marginal deformation in sequence images, there would be some overlap between the two. We term these contour pairs 'related contours'.
- At this stage, for every vertex v_i, there are n number of direction vectors D_{ij}. Following each D_{ij}, a corresponding point m_{ij} could be detected on c_d. Let us define $p(v_i, m_{ij})$ as the path to be tracked between v_i (on source c_r) and m_{ij} (on destination c_d). Even if there could be n number of such paths (as there are n number of D_{ij}), only one of them is the correct path to be established.
- Our shape-based measure considers each of these paths $p(v_i, m_{ij})$ individually following which we construct a deformed source contour between v_{i-1} and v_{i+1}. This construction is based on the qualitative assessment of curvatures between the source and the destination contour. Note that there will be n such deformed contours (as there are n number of paths $p(v_i, m_{ij})$). These deformed contours are compared with the destination contour between I_{i-1} and I_{i+1} for best matching. The optimum path $p(v_i, m_{ij})$ is the one which provides the best match between the deformed source contour D_s and the destination contour c_d.

$$p^{\text{opt}}(v_i, m_{ij}) = \min_n \int (D_s|_{v_{i-1}}^{v_{i+1}} - c_d|_{I_{i-1}}^{I_{i+1}})\, dl. \quad (5)$$

- Construction of a deformed source contour: Let us consider the source contour to be a perfectly flexible string fixed at both ends (v_{i-1} and v_{i+1} in this case). Over the period of observation δt, the displacement at v_i is known considering the corresponding point m_{ij} at the destination contour. Therefore, the tension at the string position v_i is known for any particular direction vector D_{ij}. Let this tension be F_{ij}. At the close neighbourhood of v_i, the tension in the string is calculated based on the value of F_{ij}. In the absence of any other force system, the effect of F_{ij} should decrease as we move away from v_i. However, we either decrease or increase the tension at the neighbourhood comparing curvatures between corresponding parts of related contours (Figure 2 *b*). For a neighbourhood dl (along arclength) around v_i, the derived tension of the string at $(v_i + \delta l)$, $F_{l+\delta l}$, is given as follows:

$$\begin{aligned} &\text{for } (\kappa_s - \kappa_d)|_{dl} = 0, \quad F_{v_i+\delta l} = F_{ij}, \\ &\quad (\kappa_s - \kappa_d)|_{dl} < 0, \quad F_{v_i+\delta l} = F_{ij}(1+\Delta\kappa), \\ &\quad (\kappa_s - \kappa_d)|_{dl} > 0, \quad F_{v_i+\delta l} = F_{ij}(1+\Delta\kappa). \end{aligned} \quad (6)$$

κ_s and κ_d stand for curvatures of the source and destination contours along arclength dl. The weight $\Delta\kappa$ is to boost or reduce the tension in the string:

$$\Delta\kappa = \frac{1}{v}\left|\frac{\kappa_s - \kappa_d}{\kappa_s + \kappa_d}\right|. \quad (7)$$

Since the string is fixed at both ends, for every tension at v_i, there would be opposing forces at v_{i-1} and v_{i+1}. Factor v, the damping coefficient, should take care of this. From the derived force at $(v_i + \delta l)$, the displacement at $(v_i + \delta l)$ is calculated parallel to the tension F_{ij} at v_i. The process is repeated for all 'snaxels' to cover the entire arclength between v_{i-1} and v_{i+1} to construct the deformed source contour.

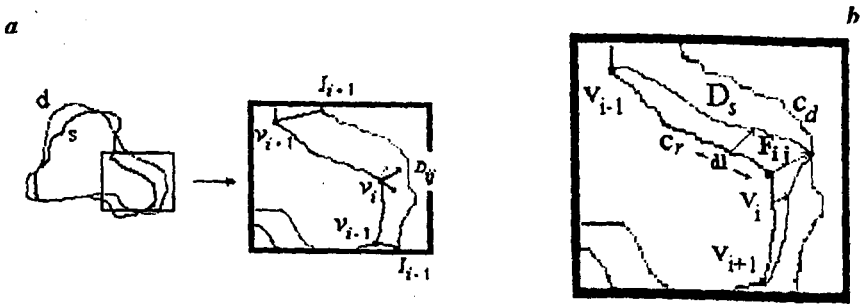

Figure 2. *a*, The source and destination contours *s* and *d* are shown along with vertices. The possible directional vectors D_{ij} are shown on the vertex v_i. *b*, Construction of deformed source contour D_s is shown between the source and the destination contour.

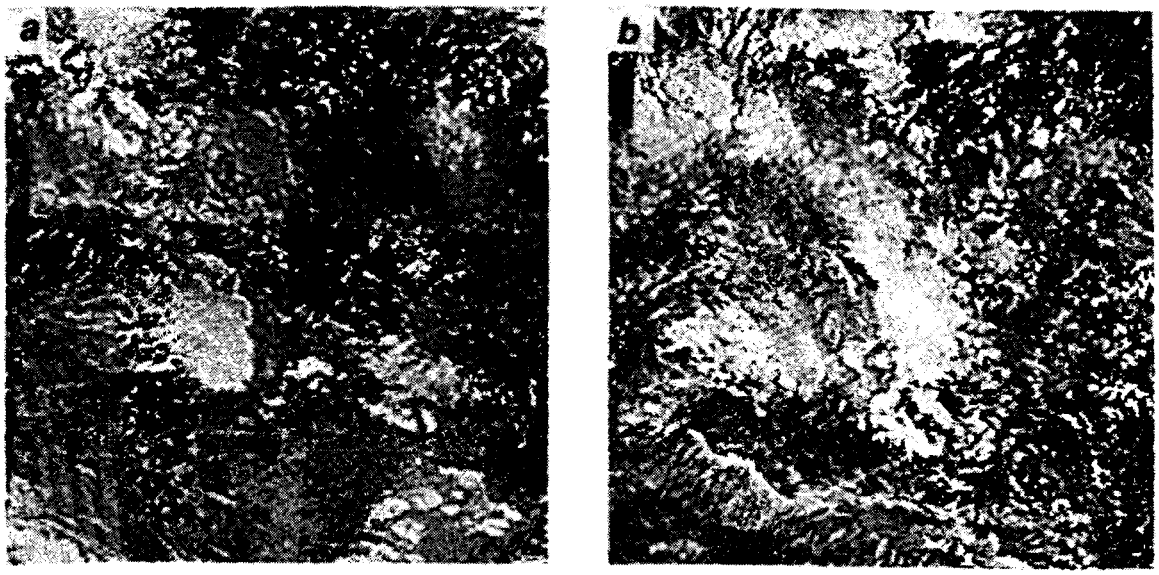

Figure 3. The source (IR) images of INSAT 1D (200 × 200 pixels) cropped out from full disk images of earth (1024 × 1024 pixels).

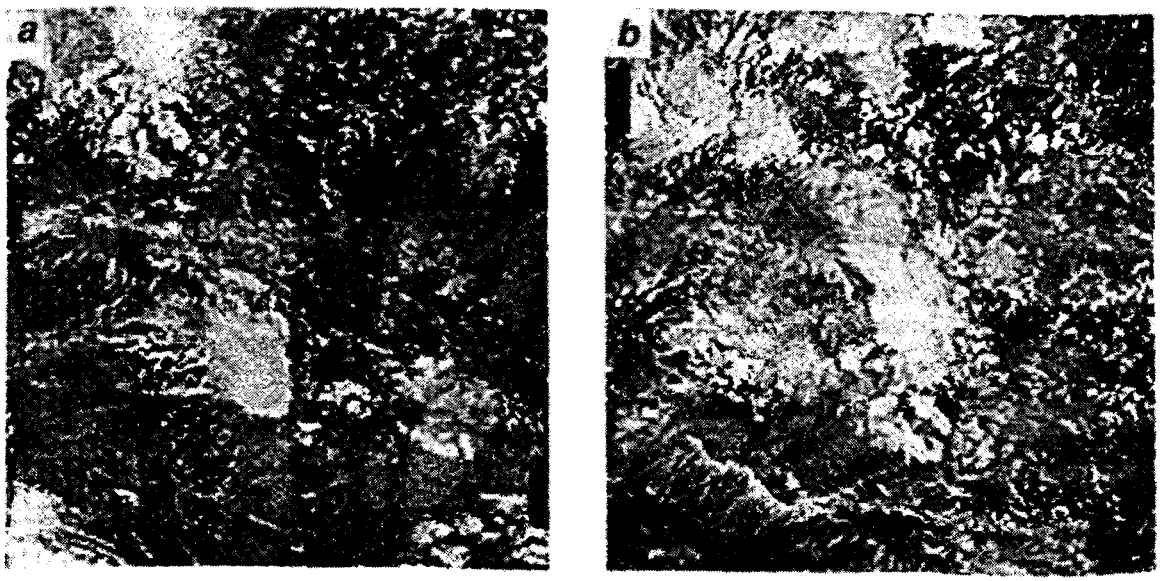

Figure 4. The destination (IR) images corresponding to source images of Figures 3 *a* and *b* respectively are shown.

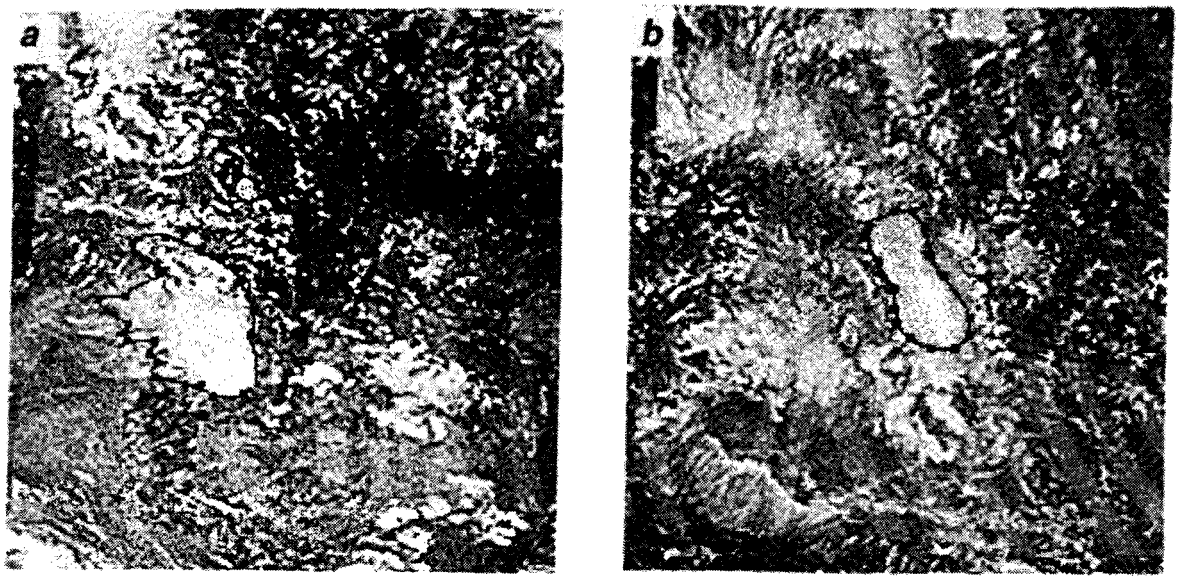

Figure 5. *Snakes* fitted to regions of interest in tracer clouds of Figures 3 *a* and *b* respectively are shown. The black square boxes represent significant points on the *snake*.

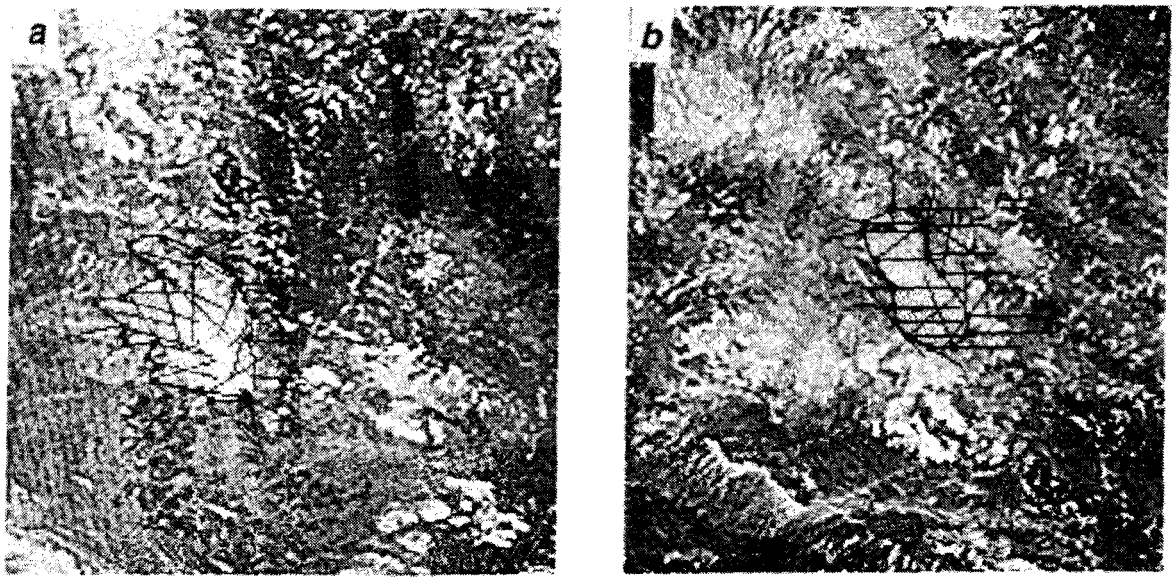

Figure 6. Initial estimates of cloud motion vectors are calculated on source images following eq. (4). For clarity of display, all direction vectors with correlation value > 0.8 are discarded.

Results

The proposed method was tested on a number of image sequences of INSAT and GMS. Two sets of results are presented in this section. Tracer cloud images are taken from INSAT 1D at 05:00 and 05:30 GMT. Figures 3 *a*, *b* and 4 *a*, *b* are the corresponding source and destination (IR) image pairs respectively. These images are registered to same scale and cropped out from full disk images of Earth. *Snakes* fitted to regions of interest on tracer clouds of source images are shown along with significant points in Figures 5 *a* and *b*. The result after initial estimates of cloud

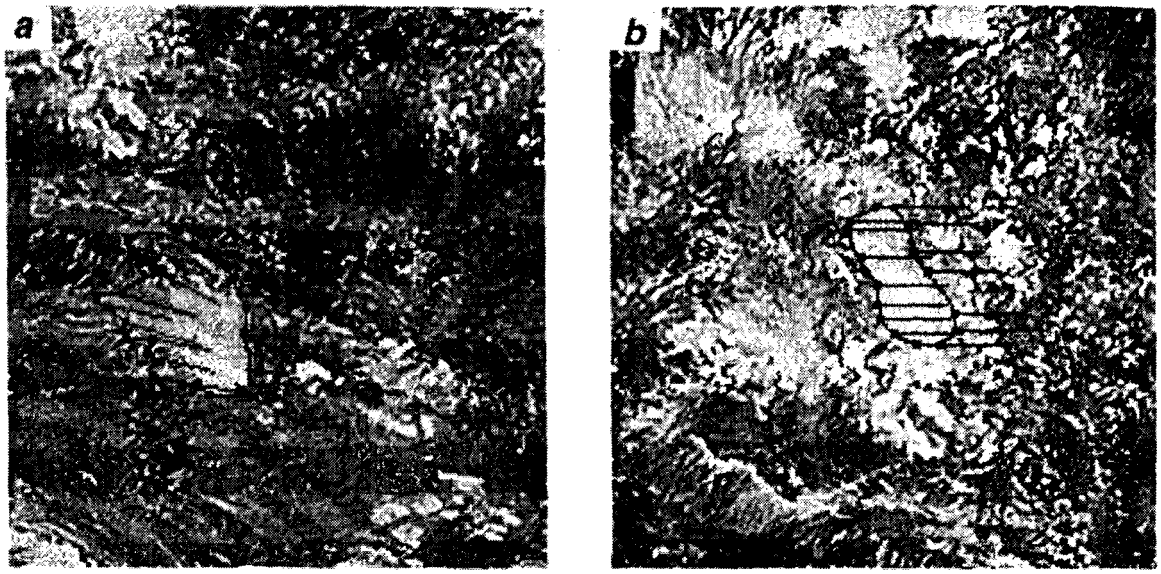

Figure 7. Optimum paths along which the significant points of source contours have moved are shown.

motion vectors following eq. (4) is shown in Figure 6. Note that the size of candidate subimage in source is taken as 15×15 pixels while the window size in destination image is taken as 37×37 pixels (V_m of w_d). For clarity of display, all direction vectors with correlation value > 0.8 are discarded. Multiple direction vectors at the vertices justify the multimodal nature of correlation surface between the source subimage and destination search window. Clearly some of the these directions do not conform to the possible movement of the cloud mass.

The optimum path $p(v_i, m_{ij})$ corresponding to the best match between the destination contour and deformed source contour sets is shown in Figure 7 *a* and *b*. To calculate the deformed contour, the curvatures between related contours are compared on every 5-pixels long arclength (dl). The tension is calculated at every third pixel (δl) of dl within the span of v_{i-1} and v_{i+1}, and the damping coefficient ν is taken as 0.5. The matching between deformed source contour and destination contour is based on the sum of squared Euclidean distance between sampled (every third) points on related contours. These points are taken starting from v_i and m_{ij} of source and destination contours respectively and moving along both directions of the curve.

Discussion

This paper presents a combined approach of intensity and shape-based methods in tracking meteorological structures. This certainly has an edge over either the gradient or the shape-based approach applied individually. At the same time it opens up several new research issues associated with the study of deformable shape. The operational procedures of CMV are restricted to a pair of sequence images. Incorporating a few more sequence images should help implement a 'predictor–corrector' scheme in estimating cloud motion. In our shape-based approach, cloud contour is modelled as a perfectly flexible string, and the local computation approach is restricted within a segment bounded by three consecutive vertices. This scheme could be upgraded considering the directional vectors at the neighbouring vertices which are not considered at present.

1. Bader, M. J., Forbes, G. S., Grant, J. R., Lilley, R. B. E. and Waters, A. J., *Images in Weather Forecasting: A Practical Guide for Interpreting Satellite and Radar Imagery*, Cambridge University Press, 1995.
2. Proceedings of the First International Wind Workshop, EUMETSAT, Washington DC, 1991.
3. Proceedings of the Second International Wind Workshop, EUMETSAT, Tokyo, Japan, 1993.
4. Berrior, J. P., Herlin, I. and Cohen, I., Proceedings of the International Conference on Analysis and Optimization of System, Images, Wavelets and PDE's, Paris, 1996.
5. Wu, Q. X., *IEEE Trans. Pat. Anal. Mach. Intell.*, 1995, **17**, 843–853.
6. Leese, J. A. and Novak, C. S., *J. Appl. Meterol.*, 1971, **10**, 118–132.
7. Kelkar, R. R. and Khanna, P. N., *Mausam*, 1986, **37**, 495–500.
8. Young, M. T., NOAA Tech. Memo, NESS 64, National Technical Information Service, US Dept. of Commerce, Virginia, 1975, pp. 111–121.
9. Green, R., Hughes, G., Novak, C. and Schreitz, R., NOAA Tech. Memo. NESS 64, National Technical Information Service, US Dept. of Commerce, Springfield, Virginia, 1975, pp. 94–101.

10. Kelkar, R. R., Prasad, S. and Gandeswaran, S. M., *Mausam*, 1987, **38**, 197–202.
11. Velden, C. S., *Meteorol. Atmos. Phys.*, 1996, **60**, 37–46.
12. Neiman, S. J., Menzel, W. P., Hayden, C. M., Gray, D., Wanzong, S., Velden, C. S. and Daniels, *J., Bull. Am. Meteorol. Soc.*, 1997.
13. Ryan, T. W., Ph D thesis, University of Arizona, 1981.
14. Anandan, P., Ph D thesis, University of Massachusetts, 1987.
15. Singh, A., *Optic Flow Computation: A Unified Perspective*, IEEE Computer Soc. Press, 1991.
16. Hasler, A. F., Skillman, W. C. and Steranka, J., *J. Appl. Meteorol.* 1979, **18**, 1481–1489.
17. Adelson, E. H. and Bergen, J. R., J. *Opt. Soc. Am.*, 1987, **A2**, 284–299.
18. Heeger, D. J., *J. Opt. Soc. Am.*, 1987, **A2**, 1455–1471.
19. Wu, Q. X., Pairman, D. and Barnes, E. J., Proceedings of the First Pacific Ocean Remote Sensing Conference, Okinawa, Japan, 1992, pp. 802–807.
20. Agarwal, J. K. and Nandhakumar, N., *IEEE. Proc.*, 1988, 76.
21. Rosenfeld, A. and Kak, A., *Digital Picture Processing*, Academic Press, New York, 2nd edn, 1982, vol. 2.
22. Kass, M., Witkin A. and Terzopoulos, D., Proceedings of First International Conference on Computer Vision, ICCV '87, 1987, pp. 259–269.
23. Cohen, L. D. and Cohen, I., *IEEE Trans. Pat. Anal. Mach. Intell.*, 1993, **15**, 1131–1147.
24. Lai, K. F., Ph D thesis, University of Wisconsin-Madison, 1994.
25. Lai, K. F. and Chin, R. T., *IEEE Trans. Pat. Anal. Mach. Intell.*, 1994.
26. Malladi, R., Sethian, J. A. and Vemuri, B. C., *IEEE Trans. Pat. Anal. Mach. Intell.*, 1995, **17**, 158–175.
27. Leymarie, F. and Levine, M. D., *IEEE Trans. Pat. Anal. Mach. Intell.*, 1993, **15**, 617–634.
28. Cochen, I., Ayache, N. and Sulger, P., Proceedings of the 2nd European Conference on Computer Vision, ECCV '92, Santa Margherita Ligure, Italy, 1992, pp. 458–466.
29. Cochen, I. and Herlin, I., Proceedings of the 6th International Conference on Computer Vision, ICCV '98, Bombay, India, 1998, pp. 396–401.
30. Kimmel, R., Amir A. and Bruckstein, A. M., *IEEE Trans. Pat. Anal. Mach. Intell.*, 1995, **17**, 635–640.
31. Rom, H. and Medioni, G., Technical Report, IRIS/91, University of Southern California, USA, 1991.

ACNOWLEDGEMENT. We thank ISRO and ASD/MOG of SAC, Ahmedabad, in particular.